

¹ **neonSoilFlux: An R Package for Continuous
2 Sensor-Based Estimation of Soil CO₂ Fluxes**

³ John Zobitz¹ Edward Ayres² Zoey Werbin³ Ridwan Abdi¹
⁴ Natalie Ashburner-Wright⁴ Lillian Brown⁴
⁵ Ryan Frink-Sobierajski⁴ Lajntxiag Lee¹ Dijonë Mehmeti¹
⁶ Christina Tran⁴ Ly Xiong¹ Naupaka Zimmerman^{4,5}

⁷ ¹ Augsburg University, 2211 Riverside Avenue, Minneapolis, MN 55454

⁸ ² National Ecological Observatory Network, Battelle, 1685 38th Street, Suite 100, Boulder, CO
⁹ 80301

¹⁰ ³ Boston University, 5 Cummington Street, Boston, MA 02215

¹¹ ⁴ University of San Francisco, 2130 Fulton Street, San Francisco, CA 94117

¹² ⁵ University of Kansas, 1450 Jayhawk Boulevard, Lawrence, KS 66045

¹³ **Acknowledgments**

¹⁴ John Zobitz acknowledges Kathleen O'Rourke for code development. Naupaka Zimmerman
¹⁵ thanks technical staff at USF for support with field gear assembly and shipping. We thank the
¹⁶ NEON field staff and assignable assets teams for facilitating each of the six NEON site visits.

¹⁷ We are grateful to LI-COR technical staff for helpful discussions about optimal soil chamber
¹⁸ sampling methods. This work was supported by NSF DEB grant #2017829 awarded to John
¹⁹ Zobitz, and NSF DEB grant #2017860 awarded to Naupaka Zimmerman. This material is
²⁰ based in part upon work supported by the National Ecological Observatory Network (NEON),
²¹ a program sponsored by the U.S. National Science Foundation (NSF) and operated under
²² cooperative agreement by Battelle. We also thank the reviewers and subject editor for their
²³ constructive feedback.

²⁴ **Conflict of Interest Statements**

²⁵ None of the authors have a financial, personal, or professional conflict of interest related to this
²⁶ work.

²⁷ **Author Contributions**

²⁸ Conceptualization: John Zobitz, Naupaka Zimmerman; Methodology: Edward Ayres, John
²⁹ Zobitz, Naupaka Zimmerman; Software: John Zobitz, Naupaka Zimmerman, Zoey Werbin,
³⁰ Edward Ayres, Dijonë Mehmeti, Ridwan Abdi, Ly Xiong, Lajntxiag Lee; Validation: John
³¹ Zobitz, Naupaka Zimmerman; Formal Analysis: John Zobitz, Naupaka Zimmerman, Dijonë
³² Mehmeti, Ridwan Abdi, Ly Xiong, Lajntxiag Lee; Investigation: John Zobitz, Naupaka Zimmerman,
³³ Ryan Frink-Sobierajski, Christina Tran, Natalie Ashburner-Wright, Lillian Brown;
³⁴ Resources: John Zobitz, Naupaka Zimmerman; Data curation: John Zobitz, Naupaka Zimmerman,
³⁵ Dijonë Mehmeti, Ly Xiong; Writing – original draft: John Zobitz, Naupaka Zimmerman;
³⁶ Writing – review and editing: John Zobitz, Naupaka Zimmerman, Zoey Werbin, Edward Ayres,
³⁷ Christina Tran, Dijonë Mehmeti, Ly Xiong; Visualization: John Zobitz, Naupaka Zimmerman,

³⁸ Dijonë Mehmeti, Ridwan Abdi, Ly Xiong; Supervision: John Zobitz, Naupaka Zimmerman;
³⁹ Project Administration: John Zobitz, Naupaka Zimmerman; Funding Acquisition: John Zobitz,
⁴⁰ Naupaka Zimmerman.

⁴¹ **Data Availability**

⁴² Anonymous field-collected data, `neonSoilFlux` calculated outputs, and manuscript-generating
⁴³ code for peer review are provided as supplemental files. An anonymous link for peer-review
⁴⁴ is here: <https://doi.org/10.5281/zenodo.1695117>. This will be made publicly available upon
⁴⁵ publication.

46 **1 Abstract**

- 47 1. Accurate quantification of soil carbon fluxes is essential to reduce uncertainty in estimates
48 of the terrestrial carbon sink. However, these fluxes vary over time and across ecosystem
49 types and so it can be difficult to estimate them accurately across large scales. The flux
50 gradient method estimates soil carbon fluxes using co-located measurements of soil CO₂
51 concentration, soil temperature, soil moisture, and other soil properties. The National
52 Ecological Observatory Network (NEON) provides such data across 20 ecoclimatic domains
53 spanning the continental U.S., Puerto Rico, Alaska, and Hawai‘i.
- 54 2. We present an R software package (`neonSoilFlux`) that acquires soil environmental data
55 to compute half-hourly soil carbon fluxes for each soil replicate plot at a given terrestrial
56 NEON site. To assess the computed fluxes, we visited six focal NEON sites and measured
57 soil carbon fluxes using a closed-dynamic chamber approach.
- 58 3. Outputs from the `neonSoilFlux` showed agreement with measured fluxes (R^2 between
59 measured and `neonSoilFlux` outputs ranging from 0.04 to 0.81 depending on calculation
60 method used); measured outputs generally fell within the range of calculated uncertainties
61 from the gradient method. Calculated fluxes from `neonSoilFlux` aggregated to the daily
62 scale exhibited expected site-specific seasonal patterns.
- 63 4. While the flux gradient method is broadly effective, its accuracy is highly sensitive
64 to site-specific inputs, including the extent to which gap-filling techniques are used to
65 interpolate missing sensor data and to estimates of soil diffusivity and moisture content.
66 Future refinement and validation of `neonSoilFlux` outputs can contribute to existing
67 databases of soil carbon flux measurements, providing near real-time estimates of a critical
68 component of the terrestrial carbon cycle.

⁶⁹ **1.1 Keywords**

⁷⁰ Soil carbon, carbon dioxide, flux gradient, carbon cycle, field validation, soil respiration,
⁷¹ ecosystem variability, diffusion

⁷² **2 Data for peer review**

⁷³ Anonymous field-collected data, `neonSoilFlux` calculated outputs, and manuscript-generating
⁷⁴ code for peer review are provided as supplemental files. An anonymous link for peer-review
⁷⁵ is here: <https://doi.org/10.5281/zenodo.16951117>. This will be made publicly available upon
⁷⁶ publication.

⁷⁷ **3 Introduction**

⁷⁸ Soils contain the planet's largest reservoir of terrestrial carbon (Jobbágy & Jackson, 2000). A
⁷⁹ critical component of this reservoir is soil organic matter, the accumulation of which is influenced
⁸⁰ by biotic factors such as above-ground plant inputs (Jackson et al., 2017). These inputs in
⁸¹ turn are influenced by environmental factors such as growing season length, temperature, and
⁸² moisture (Desai et al., 2022), which also affect the breakdown of soil organic matter and its
⁸³ return to the atmosphere. Across heterogeneous terrestrial landscapes, the interplay between
⁸⁴ these biotic and abiotic factors influence the size of the soil contribution to the terrestrial
⁸⁵ carbon sink (Friedlingstein et al., 2025). However, the heterogeneity of these processes across
⁸⁶ diverse ecosystems in the context of rapid environmental change leads to large uncertainty
⁸⁷ about the magnitude of this sink in the future, and thus there remains a pressing need to
⁸⁸ quantify changes in soil carbon pools and fluxes across scales.

89 Ecological observation networks such as the United States' National Ecological Observatory
90 Network (NEON) and others (e.g. the globally-distributed FLUXNET or the European Inte-
91 grated Carbon Observation System) present a significant advancement in the nearly continuous
92 observation of biogeochemical processes at the continental scale. Notably, at 47 terrestrial
93 sites across the continental United States that span 20 ecoclimatic domains, NEON provides
94 half-hourly measurements of soil CO₂ concentration, temperature, and moisture at different
95 vertical depths. Each of these NEON sites also encompasses measurements of the cumulative
96 sum of all ecosystem carbon fluxes in an airshed using the eddy covariance technique (Baldocchi,
97 2014). Soil observations provided by NEON are on the same timescale and standardized with
98 eddy covariance measurements from FLUXNET. These types of nearly continuous observational
99 data (NEON and FLUXNET) can be used to reconcile differences between model-derived
100 or data-estimated components of ecosystem carbon flux (Jian et al., 2022; Luo et al., 2011;
101 Phillips et al., 2017; J. Shao et al., 2015; P. Shao et al., 2013; Sihi et al., 2016).

102 Estimated or observed soil carbon fluxes are a key metric for understanding change in soil
103 carbon pools over time (Bond-Lamberty et al., 2024). A soil carbon flux to the atmosphere (F_S ,
104 units $\mu\text{mol m}^{-2} \text{s}^{-1}$), represents the aggregate process of transfer of soil CO₂ to the atmosphere
105 from physical and biological processes (e.g. diffusion and respiration). Soil carbon fluxes can
106 be assumed to encompass soil carbon respiration from autotrophic or heterotrophic sources
107 (Davidson et al., 2006) and modeled with a exponential Q_{10} paradigm (Bond-Lamberty et al.,
108 2004; Chen & Tian, 2005; Hamdi et al., 2013).

109 One common method by which F_S is measured in the field is through the use of soil chambers
110 in a closed, well-mixed system (Norman et al., 1997) with headspace trace gas concentrations
111 measured with an infrared gas analyzer (IRGA). F_S can also be estimated from soil CO₂
112 measurements at different depths in the soil using the flux-gradient method (Maier & Schack-
113 Kirchner, 2014). Closed-chamber IRGA measurements, while being the most common method,

114 require either frequent in-person site visits or expensive and fragile automated systems. The
115 potential of the gradient method is that fluxes can be estimated from continuous data recorded
116 by robust solid-state sensors. The flux-gradient method is an approach that uses conservation of
117 mass to calculate flux at a vertical soil depth z at steady state by applying Fick's law of diffusion.
118 A simplifying assumption for the flux-gradient method is that there is no mass transfer in the
119 other spatial dimensions x and y (Maier & Schack-Kirchner, 2014). The diffusivity profile, a
120 key component of this calculation, varies across the soil depth as a function of soil temperature,
121 soil volumetric water content, atmospheric air pressure, and soil bulk density (Millington &
122 Shearer, 1971; Moldrup et al., 1999; Sallam et al., 1984).

123 Databases such as the Soil Respiration Database (SRDB) or the Continuous Soil Respiration
124 Database (COSORE) add to the growing network of resources for making collected observations
125 of soil fluxes available to other researchers (Bond-Lamberty, 2018; Bond-Lamberty et al., 2020;
126 Bond-Lamberty & Thomson, 2010; Jian et al., 2021; Jiang et al., 2024). However, these
127 databases currently encompass primarily direct soil measurements of fluxes (i.e. those using
128 methods like the closed-chamber method described above). Currently, NEON provides all
129 measurements to calculate F_S from Fick's law, but soil flux as a derived data product was
130 descoped from the initial network launch due to budget constraints (Berenbaum et al., 2015).
131 Deriving estimates of F_S using continuous sensor data across NEON sites using NEON data
132 thus remains a high priority.

133 This study describes an R software package, `neonSoilFlux`, that computes a standardized
134 estimate of F_S at all terrestrial NEON sites using the flux-gradient method. Using direct
135 chamber-based field observations of soil carbon dioxide flux from a subset of terrestrial NEON
136 sites spanning six states, we provide a direct validation of F_S from `neonSoilFlux`. While
137 open source R software tools currently exist for processing chamber-based flux measurements
138 (Jurasinski et al., 2022; Pedersen, 2024; Rheault et al., 2024; Wilson et al., 2024; Zhao, 2019),

¹³⁹ to our knowledge this is the first package that incorporates NEON data directly.

¹⁴⁰ Key objectives of this study are to:

- ¹⁴¹ 1. Apply the flux-gradient method to estimate soil CO₂ flux from continuous sensor mea-
- ¹⁴² surements across six NEON sites.
- ¹⁴³ 2. Benchmark estimated soil carbon fluxes against field measurements (e.g. direct chamber
- ¹⁴⁴ measurements of soil flux).
- ¹⁴⁵ 3. Identify sources of error in the flux-gradient approach across diverse sites in order to
- ¹⁴⁶ guide future work.

¹⁴⁷ **4 Materials and Methods**

¹⁴⁸ **4.1 Field methods**

¹⁴⁹ **4.1.1 Focal NEON Sites**

¹⁵⁰ In order to acquire field data to validate model predictions of flux, we selected six terrestrial
¹⁵¹ NEON sites for analysis. We conducted roughly week-long field measurement campaigns at
¹⁵² these sites, which span a range of environmental gradients and terrestrial domains (Table 1).
¹⁵³ SJER, SRER, and WREF were visited during May and June of 2022, and WOOD, KONZ,
¹⁵⁴ and UNDE during May and June of 2024.

¹⁵⁵ **4.1.2 Soil collar placement**

¹⁵⁶ Either one (2022 sampling campaign) or two (2024 sampling campaign) PVC soil collars (20.1
¹⁵⁷ cm inside diameter) were installed in close proximity to the permanent NEON soil sensors at

158 each site (Figure 1). As instruments in the NEON soil sensor arrays can occasionally break
159 down or stop working, the specific soil plot where we made measurements was chosen at each
160 site in consultation with NEON staff to maximize likelihood of quality soil sensor measurements
161 during the duration of the IRGA measurements. The plot selected at each site (out of the 5 in
162 each replicate array at each site) are presented in the last column of Table 1. After installation,
163 collar(s) were left to equilibrate for approximately 24 hours prior to any measurements being
164 taken.

165 **4.1.3 Infrared gas analyzer measurements of soil CO₂ flux**

166 In 2022, we then made measurements of flux on an hourly interval for 8 hours each day.
167 Measurements were taken from roughly 8 am to 4 pm, with the time interval selected to
168 capture the majority of the diurnal gradient of soil temperature each day. These measurements
169 were made using a LI-6800 infrared gas analyzer instrument (LI-COR Environmental, Lincoln,
170 NE) fitted with a soil chamber attachment (attachment 6800-09). In 2024, we again used the
171 same LI-6800 instrument, but made half-hourly measurements over an approximately 8 hour
172 period. In addition, in 2024 we also installed a second collar and used a second instrument, an
173 LI-870 CO₂ IRGA, connected to an automated robotic chamber (LI-COR chamber 8200-104)
174 controlled by an LI-8250 multiplexer to make automated measurements. The multiplexer was
175 configured to take half-hourly measurements 24 hours a day for the duration of our sampling
176 bout at each site. Each instrument was paired with a soil temperature and moisture probe
177 (Stevens HydraProbe, Stevens Water, Portland, OR) that was used to make soil temperature
178 and moisture measurements concurrent with the CO₂ flux measurements. Chamber volumes
179 were set by measuring collar offsets at each site. System checks were conducted daily for the
180 LI-6800 and weekly for the LI-8250. Instruments were factory calibrated before each field
181 season.

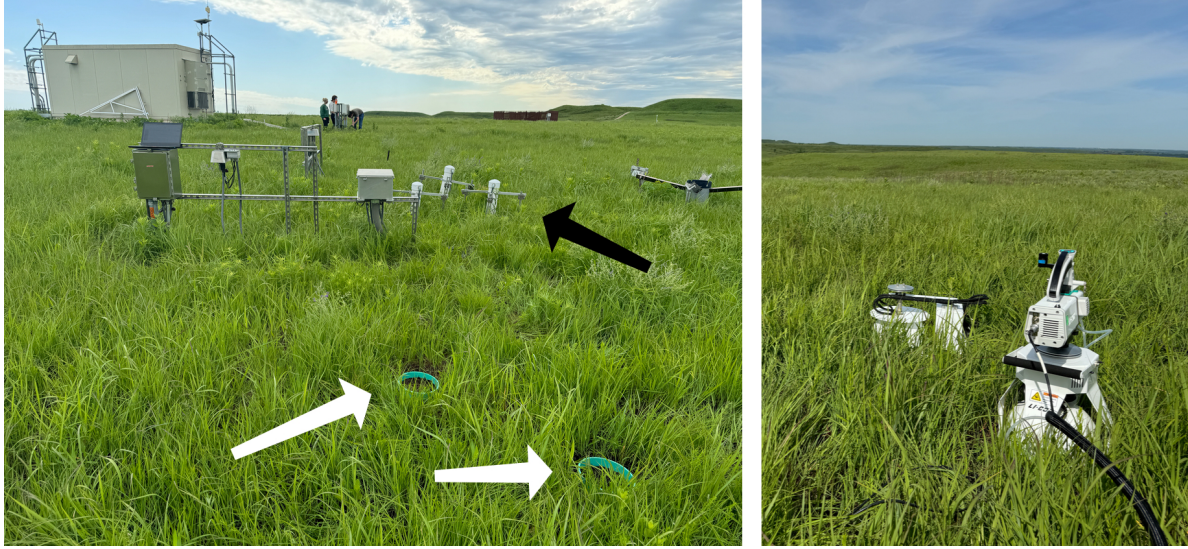


Figure 1: Spatial layout of field sampling using a closed-dynamic chamber setup at a representative NEON site (KONZ). Left image shows collars (white arrows) and permanent soil sensor installation (black arrow) and right image shows the LI-6800 (foreground) and LI-8200-104 (background) instruments placed on the collars.

Table 1: Listing of NEON sites studied for field work and analysis. Site refers to NEON site codes: Santa Rita Experimental Range (SRER), San Joaquin Experimental Range (SJER), Wind River Experimental Forest (WREF), Chase Lake National Wildlife Refuge (WOOD), Konza Prairie Biological Station (KONZ), and the University of Notre Dame Environmental Research Center (UNDE). Location is reported in decimal degrees of latitude and longitude. Other abbreviations include Mean Annual Temperature (MAT); $\overline{T_S}$: average soil temperature during field measurements; \overline{SWC} : average soil water content during field measurements. Dates refer to field measurement dates for each site. Plot refers to the particular location in the soil sensor array (denoted as HOR by NEON) where field measurements were made.

Site	Location	Ecosystem	MAT	$\overline{T_S}$	MAP	\overline{SWC}	Dates	Plot
SRER	31.91068, -110.83549	Shrubland	19.3 °C	47.6 °C	346 mm	4.0%	May 29– June 1 2022	004
SJER	37.10878, -119.73228	Oak woodland	16.4 °C	41.7 °C	540 mm	1.2%	June 1–4 2022	005
WREF	45.82049, -121.95191	Evergreen forest	9.2 °C	15.3 °C	2225 mm	27.2%	June 7–9 2022	001
WOOD	47.1282, -99.241334	Restored prairie	4.9 °C	14.9 °C	495 mm	14.9%	June 3–9 2024	001
KONZ	39.100774, -96.563075	Tallgrass prairie	12.4 °C	23.4 °C	870 mm	23.4%	May 29– June 1 2024	001

Table 1: Listing of NEON sites studied for field work and analysis. Site refers to NEON site codes: Santa Rita Experimental Range (SRER), San Joaquin Experimental Range (SJER), Wind River Experimental Forest (WREF), Chase Lake National Wildlife Refuge (WOOD), Konza Prairie Biological Station (KONZ), and the University of Notre Dame Environmental Research Center (UNDE). Location is reported in decimal degrees of latitude and longitude. Other abbreviations include Mean Annual Temperature (MAT); \bar{T}_S : average soil temperature during field measurements; \bar{SWC} : average soil water content during field measurements. Dates refer to field measurement dates for each site. Plot refers to the particular location in the soil sensor array (denoted as HOR by NEON) where field measurements were made.

Site	Location	Ecosystem	MAT	\bar{T}_S	MAP	\bar{SWC}	Dates	Plot
UNDE	46.23391, -89.537254	Deciduous forest	4.3 °C	13.0 °C	802 mm	13.0%	May 22–25 2024	004

182 4.1.4 Post-collection processing of field data

183 We used LI-COR SoilFluxPro software (v 5.3.1) to assess the data after collection and to
 184 inform sampling parameters. We checked appropriateness of dead band and measurement
 185 durations using built-in evaluation tools. Based on this, the deadband period was set for 30-40
 186 seconds, depending on the site, and the measurement duration was 180 seconds with a 30
 187 second pre-purge and a 30 second post-purge at most sites, and a 90 second pre- and post-purge
 188 at sites with higher humidity due to recent precipitation events. We also assessed the R^2 of
 189 linear and exponential model fits to measured CO₂ to verify measurement quality.

190 4.2 neonSoilFlux R package

191 We developed an R package called `neonSoilFlux` (Zobitz et al., 2024) to compute half-hourly
 192 soil carbon fluxes and uncertainties from NEON data. The objective of the `neonSoilFlux`
 193 package is a unified workflow (Figure 2) for soil data acquisition and analysis that supplements
 194 the existing `neonUtilities` data acquisition R package (Lunch et al., 2025).

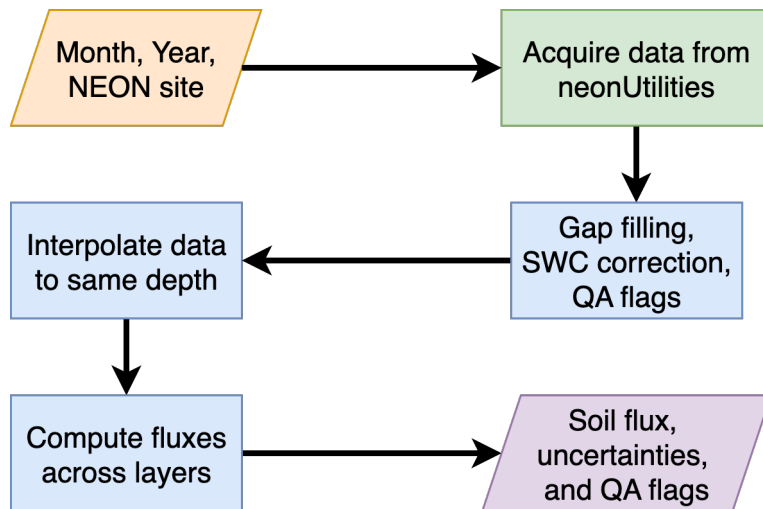


Figure 2: Diagram of `neonSoilFlux` R package. For a given month, year, and NEON site (orange parallelogram), the package acquires all relevant data to compute F_S using the `neonUtilities` R package (green rectangle). Data are gap-filled according to reported QA flags and adjusted for changes in soil water content (SWC) calibration coefficients, then interpolated to the same measurement depth before computing the soil flux, uncertainties, and final QA flags (blue rectangles). The package reports the associated soil flux, uncertainties, and quality assurance (QA) flags for the user (purple parallelogram).

195 At a given NEON site there are five replicate soil plots, each with measurements of soil
 196 CO_2 concentration, soil temperature, and soil moisture at different depths (Figure 3). The
 197 `neonSoilFlux` package acquires measured soil CO_2 concentration (NEON, 2024b), soil temper-
 198 ature (NEON, 2024d), soil water content (NEON, 2024e), barometric pressure from the nearby
 199 tower (NEON, 2024a), and soil properties (e.g. bulk density) (NEON, 2024c) from a range of
 200 different NEON data products. The static soil properties were collected by NEON staff from a
 201 nearby soil pit during initial site characterization and are assumed to be constant at each site.
 202 A soil flux calculation is computed at each replicate soil plot.

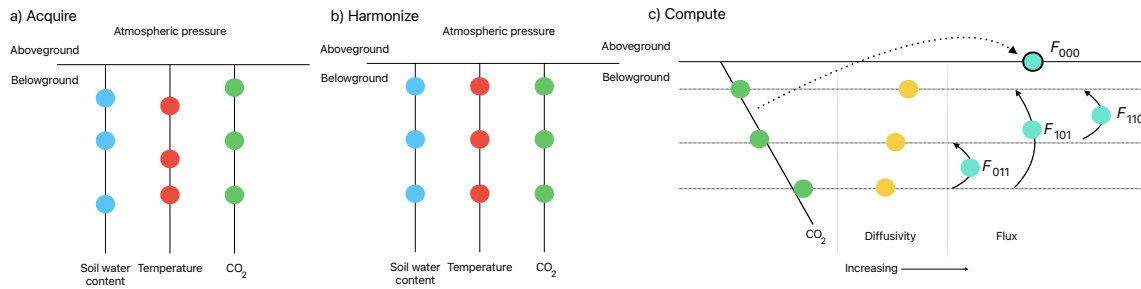


Figure 3: Model diagram of the data workflow for the `neonSoilFlux` R package. a) Acquire: Data are obtained for a given NEON location and horizontal sensor location, which includes soil water content, soil temperature, CO_2 concentration, and atmospheric pressure. All data are screened for quality assurance; if gap-filling of missing data occurs, it is flagged for the user. b) Harmonize: Any belowground data are then harmonized to the same depth as CO_2 concentrations using linear regression. c) Compute: The flux across a given depth is computed via Fick's law, denoted with F_{ijk} , where i , j , or k are either 0 or 1 denoting the layers the flux is computed across (i = closest to surface, k = deepest). F_{000} represents a flux estimate where the gradient dC/dz is the slope of a linear regression of CO_2 with depth.

203 The workflow to compute a value of F_S with `neonSoilFlux` consists of three primary steps,
 204 illustrated in Figure 3. First, NEON data are acquired for a given site and month via the
 205 `neonUtilities` R package (yellow parallelogram and green rectangle in Figure 2 and Panel a
 206 in Figure 3). Acquired environmental data can be exported to a comma separated value file for
 207 additional analysis. Quality assurance (QA) flags are reported as an indicator variable. Since

208 the calibration coefficients on the soil water content sensors have changed over time (NEON,
209 2024e), raw sensor measurements were back-calculated and soil-specific calibrations were applied
210 following Ayres et al. (2024) to generate a consistent time series at each measurement location.

211 The second step is harmonizing the data to compute soil fluxes across soil layers. This
212 step consists of three different actions (blue rectangles in Figure 2 and Panel b in Figure 3).
213 If a given observation by NEON is reported as not passing a quality assurance check, we
214 applied a gap filling method to replace that measurement with its monthly mean at that same
215 depth (Section 4.2.1). Belowground measurements of soil water and soil temperature are then
216 interpolated to the same depth as soil CO₂ measurements. The diffusivity (Section 4.2.2) and
217 soil flux across different soil layers (Section 4.2.3) are then computed.

218 The third and final step is computing a surface soil flux through extrapolation to the surface
219 (purple parallelogram in Figure 2 and Panel c in Figure 3). Uncertainty on a soil flux
220 measurement is computed through quadrature. An aggregate quality assurance (QA) flag for
221 each environmental measurement is also reported, representing if any gap-filled measurements
222 were used in the computation of a soil flux. Within the soil flux-gradient method, several
223 different approaches can be used to derive a surface flux (Maier & Schack-Kirchner, 2014); the
224 `neonSoilFlux` package reports four different possible values for soil surface flux (Section 4.2.3)
225 for each of two different methods of diffusivity estimation, for a total of eight estimates of
226 flux.

227 4.2.1 Gap-filling routine

228 NEON reports QA flags as binary values for each measurement and half-hourly interval. For a
229 given half-hour, if any input variable (soil CO₂ concentration, soil temperature, or soil moisture)
230 at depth z is flagged, computation of F_S is not possible. To address this, flagged measurements

231 and their uncertainties were replaced with a bootstrapped monthly mean (\bar{m}) and monthly
232 standard deviation (\bar{s}) (Efron & Tibshirani, 1994).

233 For each month, depth z , and variable, we computed bootstrapped estimates of \bar{m} and \bar{s}
234 from the vectors of unflagged measurements (\mathbf{m}), reported standard errors (σ), and the 95%
235 confidence interval (ϵ , or expanded uncertainty; Farrance & Frenkel (2012)). We also defined a
236 bias vector $\mathbf{b} = \sqrt{\epsilon^2 - \sigma^2}$, which quantifies the spread of uncertainty in a given period and is
237 incorporated into \bar{m} .

238 From these, 5000 bootstrap samples were generated for \mathbf{m} , σ , and \mathbf{b} . For each sample (m_k, b_k, σ_k),
239 we generated a vector \mathbf{n} (length $N = 5000$) by drawing from a normal distribution with mean
240 $m_k + b_k$ and standard deviation σ_k . The sample mean and standard deviation were then
241 computed from \mathbf{n} . The resulting distributions of sample means and sample standard deviations
242 provided the bootstrapped monthly mean (\bar{m}) and standard error (\bar{s}) respectively.

243 This gap-filling procedure provides a consistent treatment across all data streams. However,
244 alternative approaches may be better suited for longer gaps (e.g., correlations with other NEON
245 measurement levels or soil plots) or for variable-specific conditions. We discuss the effect of
246 gap-filling on our results in Section 6.1.

247 **4.2.2 Soil diffusivity**

248 Soil diffusivity D_a at a given measurement depth is the product of the diffusivity in free air
249 $D_{a,0}$ ($\text{m}^2 \text{ s}^{-1}$) and the tortuosity ξ (no units) (Millington & Shearer, 1971).

250 We compute $D_{a,0}$ with Equation 1:

$$D_{a,0} = 0.0000147 \cdot \left(\frac{T_i + 273.15}{293.15} \right)^{1.75} \cdot \left(\frac{P}{101.3} \right) \quad (1)$$

251 where T_i is soil temperature ($^{\circ}\text{C}$) at depth i (NEON, 2024d) and P surface barometric pressure
252 (kPa) (NEON, 2024a).

253 Previous studies by Sallam et al. (1984) and Tang et al. (2003) demonstrated the sensitivity
254 of modeled F_S depending on the tortuosity model (ξ) used to compute diffusivity. At low
255 soil water content, the choice of tortuosity model can lead to order-of-magnitude differences
256 in D_a , which in turn affect modeled F_S . The `neonSoilFlux` package currently includes two
257 approaches to calculate ξ , representing the range of tortuosity behavior reported in Sallam et
258 al. (1984).

259 The first approach is the Millington-Quirk model (Millington & Shearer, 1971), in which
260 tortuosity depends on both porosity and soil water content:

$$\xi = \frac{(\phi - SWC_i)^{10/3}}{\phi^2} \quad (2)$$

261 In Equation 2, SWC is the soil water content at depth i (NEON, 2024e) and ϕ is the porosity,
262 which in turn is a function of soil physical properties (NEON, 2024c):

$$\phi = \left(1 - \frac{\rho_s}{\rho_m}\right) (1 - f_V) \quad (3)$$

263 In Equation 3, ρ_m is the particle density of mineral soil (2.65 g cm^{-3}), ρ_s the soil bulk density
264 (g cm^{-3}) excluding coarse fragments greater than 2 mm (NEON, 2024c), and f_V is a site-specific
265 value that accounts for the proportion of soil fragments between 2-20 mm. Soil fragments
266 greater than 20 mm were not estimated due to limitations in the amount of soil that can be
267 analyzed (NEON, 2024c). We assume that rock fragments contain no internal pores.

268 The Millington-Quirk model assumes ξ is modulated by the amount of fluid saturation in soil
269 pores (Millington & Shearer, 1971). In contrast, the Marshall model (Marshall, 1959) expresses
270 tortuosity as only a function of porosity ($\xi = \phi^{1.5}$), with ϕ defined from Equation 3. The
271 Marshall model is independent of soil water content and assumes tortuosity is only governed
272 by soil structure. The `neonSoilFlux` package allows users to choose the tortuosity model most
273 appropriate for site-specific conditions and research goals.

274 **4.2.3 Soil flux computation**

275 We applied Fick's law (Equation 4) to compute the soil flux F_{ij} ($\mu\text{mol m}^{-2} \text{s}^{-1}$) across two soil
276 depths i and j :

$$F_{ij} = -D_a \frac{dC}{dz} \quad (4)$$

277 where D_a is the diffusivity ($\text{m}^2 \text{s}^{-1}$) and $\frac{dC}{dz}$ is the gradient of CO_2 molar concentration (μmol
278 m^{-3} , so the gradient has units of $\mu\text{mol m}^{-3} \text{m}^{-1}$). The soil surface flux is theoretically defined
279 by applying Equation 4 to measurements collected at the soil surface and directly below the
280 surface. Measurements of soil temperature, soil water content, and soil CO_2 molar concentration
281 across the soil profile allow for application of Equation 4 across different soil depths. Each
282 site had three measurement layers, so we denote the flux as a three-digit subscript F_{ijk} with
283 indicator variables i , j , and k indicate if a given layer was used (written in order of increasing
284 depth), according to the following:

- 285 • F_{000} is a surface flux estimate using the intercept of the linear regression of D_a with
286 depth and the slope from the linear regression of CO_2 with depth (which represents $\frac{dC}{dz}$

in Fick's Law). Tang et al. (2003) used this approach to compute fluxes in an oak-grass savannah.

- F_{110} is a flux estimate across the two shallowest measurement layers.
- F_{011} is a flux estimate across the two deepest measurement layers.
- F_{101} is a flux estimate across the shallowest and deepest measurement layers.

For F_{110} , F_{011} , and F_{101} , the diffusivity used in Fick's Law is always at the deeper measurement layer. When used as a surface flux estimate we assume CO₂ remains constant above this flux depth. Uncertainty in all F_{ijk} values was quantified using quadrature (Taylor, 2022). These computed fluxes could provide the basis for additional soil flux estimates. For example, Tang et al. (2005) estimated surface flux by linearly extrapolating F_{110} and F_{011} to the soil surface.

4.3 Post processing evaluation

Following collection of field measurements and calculation of the soil fluxes from `neonSoilFlux` package, we compared measured F_S based on closed-dynamic chamber measurements with the LI-COR instruments to a given soil flux calculation from `neonSoilFlux` for each site and flux computation method and quantified the relationship statistically (R^2). Finally, for a half-hourly interval we also computed a *post hoc* diffusivity (D_a) using the LI-COR flux along with the CO₂ surface gradient reported by NEON using the measurement levels closest to the surface.

Table 2: Summary of measured soil characteristics and flux results from field measurements across six NEON sites using a LI-COR 6800 (LI-870/8250 measurements omitted to enable direct comparability) via the closed-dynamic chamber method. Numeric values for soil CO₂ flux, soil temperature, and volumetric soil water content (VSWC) are the mean and standard deviation of field measurements at each site.

Site	Flux μmol m ⁻² s ⁻¹	Soil temp °C	VSWC cm ³ cm ⁻³	n
UNDE	2.55 ± 0.26	14.33 ± 0.77	0.33 ± 0.02	61
WOOD	3.02 ± 0.4	16.01 ± 1.54	0.28 ± 0.01	53
WREF	3.62 ± 0.3	15.34 ± 1.76	0.27 ± 0.06	21
KONZ	6.35 ± 0.97	27.28 ± 4.14	0.37 ± 0.01	44
SJER	0.94 ± 0.02	41.68 ± 11.22	0.01 ± 0.01	32
SRER	0.72 ± 0.09	47.64 ± 7.46	0.04 ± 0.01	32

5 Results

Concordance between modelled and measured soil CO₂ flux

The sites we visited ranged substantially in both their annual average temperature and precipitation as well as their biome type (Table 2). These differences also influenced the wide range of observed flux rates across sites.

The timeseries of the measured fluxes from the LI-COR 6800 and 870/8250 were compared to modeled soil fluxes from the `neonSoilFlux` R package (Figure 4). We also assessed year-long estimated flux time series and compared those to field measurements made at each site (Figure 5). Results are reported in local time. Where applicable, sites are displayed from left to right by increasing soil temperature (Table 1). Positive values of the flux indicate that there is a flux moving towards the surface. Overall, with the exception of SRER (discussed later) the computed fluxes determined using a variety of plausible methods spanned the field-measured fluxes, but the specific flux-gradient method that best approximated field measurements varied by site.

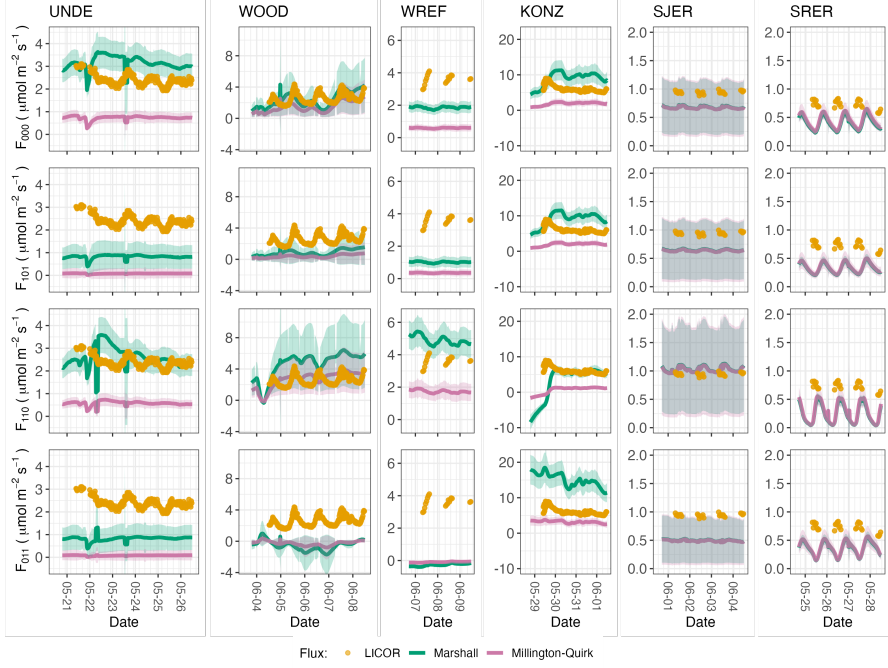


Figure 4: Timeseries of soil surface flux (F_S) from field-measured (yellow lines) and modeled soil fluxes (green or purple lines) by the `neonSoilFlux` R package. Fluxes from the `neonSoilFlux` R package are separated by the diffusivity model used (Millington-Quirk or Marshall, Section 4.2.2). Individual vertical axis labels in the first column represent the measurement levels where the flux-gradient approach is applied (Section 4.2.3). Ribbons for modeled soil fluxes represent ± 1 standard deviation. Results are reported in local time. WREF, SJER, and SRER were sampled in 2022, and UNDE, WOOD, and KONZ were sampled in 2024. Sites (columns) are arranged from left to right in terms of increasing mean annual temperature.

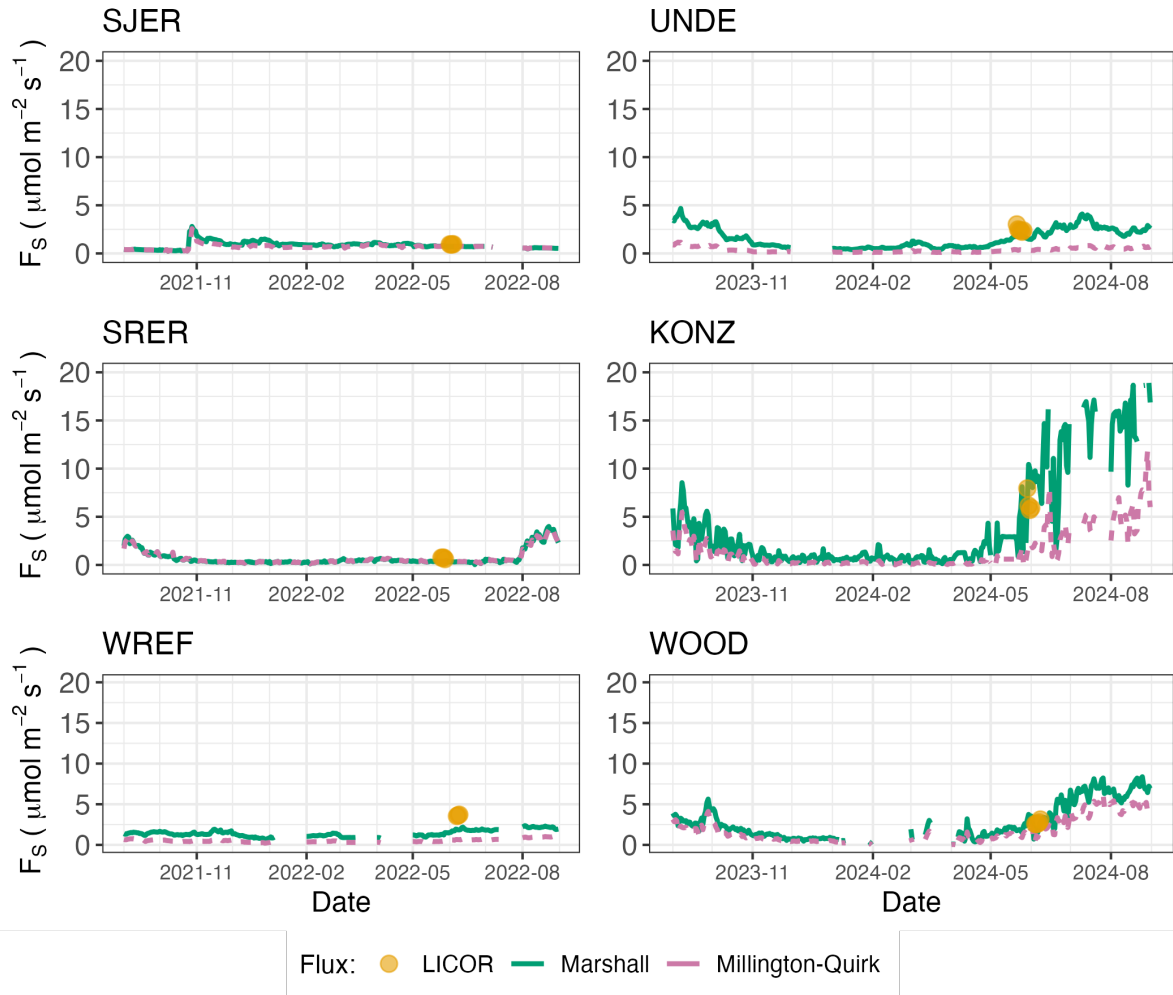


Figure 5: Timeseries of both daily-averaged field F_S (yellow circles) and daily ensemble averaged soil fluxes (average of F_{000} , F_{101} , F_{011} , F_{110} , Section 4.2.3) by the `neonSoilFlux` R package, separated by the diffusivity model used (green or purple lines, Millington-Quirk or Marshall, Section 4.2.2).

318 We calculated a statistical relationship between the various estimates of soil flux computed by
319 `neonSoilFlux` and the field-measured fluxes within daily interval periods. Statistics for these
320 comparisons are reported in Figure 6, which also shows how these fall relative to a 1:1 line.

321 **5.2 Effects of method choice on diffusivity estimates**

322 In four of six field sites, the *post hoc* D_a estimate fell roughly between the two diffusion
323 estimation methods; however this was less the case in the two driest sites, SJER and SRER
324 (Table 1), where the field estimate of diffusivity was either lower or higher than both of the
325 other methods (Figure 7).

326 **6 Discussion**

327 This study presents a unified data science workflow to efficiently process automated measure-
328 ments of belowground soil CO₂ concentrations, soil water content, and soil temperature to
329 infer estimates of soil surface CO₂ effluxes through application of Fick's Law (Equation 4).
330 Our core goals in this study were: (1) to generate estimates of soil flux from continuous soil
331 sensor data at terrestrial NEON sites using the flux-gradient method and then (2) to compare
332 those estimates to field-measured fluxes based on the closed chamber approach at six NEON
333 focal sites. We discuss our progress toward these core goals through (1) an overall evaluation
334 of the flux-gradient approach (and uncertainty calculation) and (2) site-specific evaluation of
335 differences in estimated vs measured fluxes.

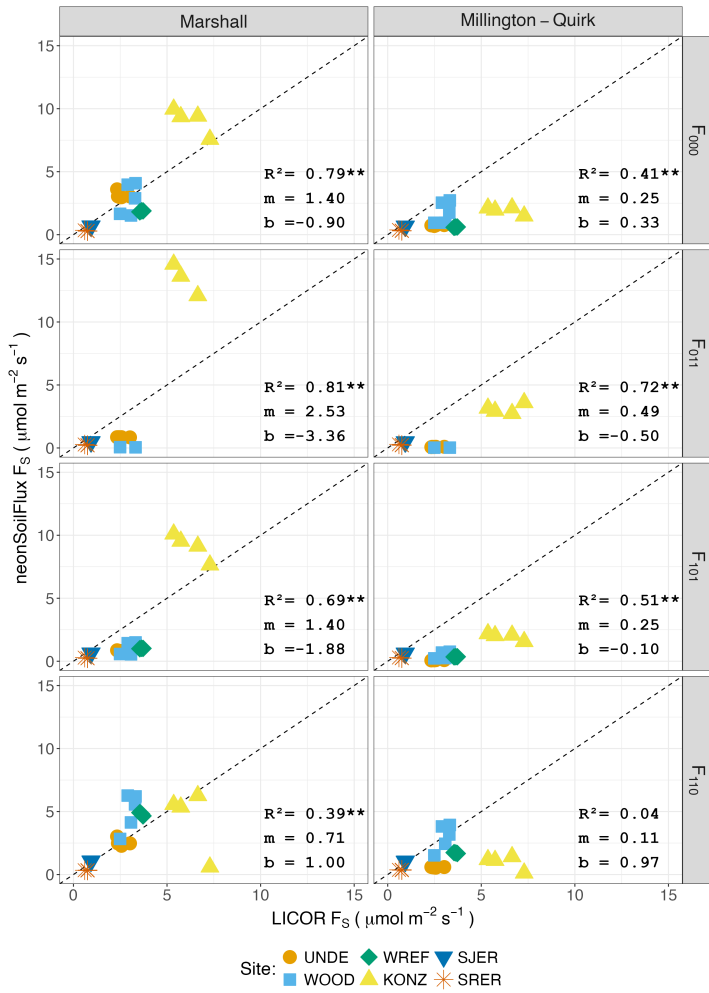


Figure 6: Statistical comparison between measured fluxes at each NEON site with fluxes reported by `neonSoilFlux` with the different flux calculation approaches and diffusivity calculations applied. Points are daily averages and LICOR F_S values are from the 6800 instrument only, for consistency. The dotted line represents a 1:1 relationship, and the reported R^2 quantifies the relationship between field-measured and `neonSoilFlux` estimated fluxes. * = significance at the 5% level, ** = significance at the 1% level. The slope (m) and intercept (b) of the linear regression between measured and modeled fluxes are also reported. The low-value outlier from KONZ in the F_{110} Marshall plot is an example of the effect of inverted CO₂ gradients causing an estimated flux to be negative, bringing down the daily mean, which later resolved as the soils dried back out.

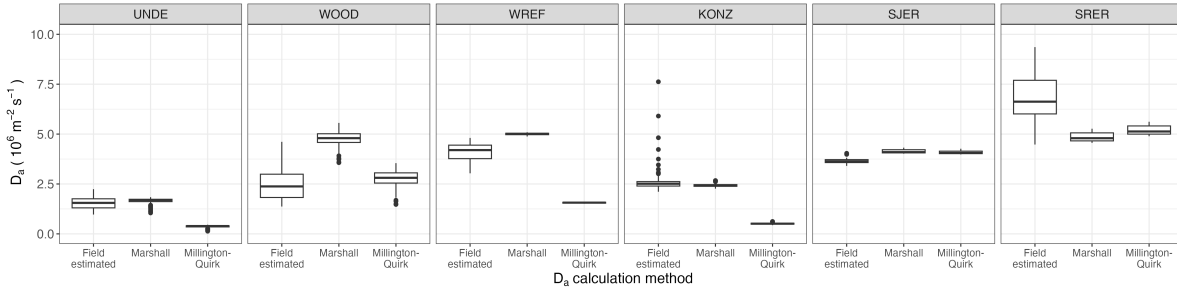


Figure 7: Distribution of diffusivity (D_a) at each study site. Values of D_a were provided by the `neonSoilFlux` package, computed from the Millington-Quirk or Marshall models (Section 4.2.2). A post-hoc estimate of diffusivity (labeled as “Field estimated”) was computed through the field measured flux (Figure 4), divided by the CO_2 gradient from the measurement levels closest to the soil surface, as reported by NEON. We only used F_S measured by the LICOR 6800 at all sites to standardize comparisons.

336 6.1 General evaluation of flux-gradient approach

337 Key assumptions of the flux-gradient approach are that CO_2 concentrations increase throughout
 338 the soil profile such that the highest concentrations are observed in the deepest layers. Addition-
 339 ally, field flux measurements should correlate with F_{000} because they represent surface fluxes.
 340 Periods where this gradient condition are not met generally are connected to processes that occur
 341 during soil wetting events, where more shallow soil layers produce higher concentrations of CO_2
 342 due to microbial respiration pulses following rewetting. This effect is likely to be largest at sites
 343 with rich organic soils (e.g. KONZ). Based on this reasoning, in these types of situations we would
 344 *a priori* expect F_{011} (deepest layers) $\leq F_{101} \leq F_{110}$ (shallow layers) $\leq F_{000}$ (all layers) be-
 345 cause the previous flux estimates rely primarily on CO_2 concentrations at deeper depths, and
 346 could miss high concentrations of CO_2 produced in shallower layers.

347 When modeling soil respiration, typically a non-linear response function that also considers soil
 348 type is used (Bouma & Bryla, 2000; Yan et al., 2016, 2018). For the `neonSoilFlux` package,
 349 soil type is connected to the measurement of bulk density, which was characterized at each
 350 NEON site. This bulk density estimate is based on replicate samples collected from the site

351 megapit at a subset of soil horizons, with an estimated uncertainty of $\pm 5\%$ (NEON, 2024c).
352 Coarse fragment estimates also have very large uncertainties, but because the volume fraction
353 tends to be low in surface soils it is unlikely to contribute much additional flux uncertainty.

354 Our results suggest that the most important way to improve reliability of the flux estimate is
355 to reduce the usage of gap-filled data. The current approach to gap filling in `neonSoilFlux`
356 uses monthly mean data to gap fill—this approach decreases the ability of the estimate to be
357 responsive to short-term pulses that occur with rapid weather shifts. Four sites (KONZ, SRER,
358 WREF, and UNDE) had more than 75% of half-hourly periods with no-gap filled measurements
359 (Figure S1, Supplementary Information). Two sites (SJER and WOOD) had more than 75% of
360 half-hourly intervals with just one gap-filled measurement. The large uncertainty evident in
361 Figure 4 for estimates from WOOD and SJER are thus due in part to the gap-filling used in
362 these sites (Figure S1). While we did not need to use gap-filled measurements to compute the
363 flux at WREF, field data collection occurred following a severe rainstorm, with soils at the
364 beginning of the sampling week near their water holding capacity. In general, we recommend
365 that whenever possible, knowledge of local field conditions should influence analysis decisions
366 in addition to any QA filtering protocols in the `neonSoilFlux` package.

367 We recognize that this gap-filling approach may lead to gap-filled values that are quite different
368 from the actual values, such as an underestimate of soil moisture following rain events. Further
369 extensions of the gap filling method could use more sophisticated gap-filling routines, similar to
370 what is used for net ecosystem carbon exchange (Falge et al., 2001; Liu et al., 2023; Mariethoz
371 et al., 2015; Moffat et al., 2007; Zhang et al., 2023). Additionally, since the deepest temperature
372 and soil moisture sensors are located below the deepest CO₂ sensors at NEON sites, it is
373 possible that excluding these deeper layers from consideration prior to analysis would lead to a
374 reduced need for gap filling. Future iterations of the `neonSoilFlux` package may incorporate
375 this as an option. The current gap-filling routine provides a consistent approach that can be

376 applied to each data stream, but further work may explore alternative gap-filling approaches.

377 **6.2 Evaluation of flux-gradient approach at each site**

378 Derived results from the `neonSoilFlux` package have patterns that are broadly consistent with
379 those directly measured in the field (Figure 4 and Figure 5), even though statistical comparisons
380 between the field-measured and `neonSoilFlux` values were quite variable (e.g. R^2 ranging
381 from 0.04 to 0.81; Figure 6). One advantage of the `neonSoilFlux` package is its ability to
382 calculate fluxes across different soil depths (Figure 3), which allows for additional site-specific
383 customization. We believe the package can provide a useful baseline estimate of soil fluxes that
384 can always be complemented through additional field measurements.

385 The six locations studied provide a range of case studies that suggest different considerations
386 may apply to different sites when applying the flux-gradient method. For example, the Santa
387 Rita Experimental Range (SRER) is a desert site characterized by sandy soil, which also was
388 the location of the highest field soil temperatures that we observed (Table 2). At SRER the
389 flux across the top two layers (F_{110}) produced a pattern of soil flux most consistent with the
390 observed field data. The remaining methods F_{101} , F_{011} , or F_{000} are derived from information
391 taken from the deepest layer, which seems to have been decoupled from the surface layers both
392 in terms of temperature and CO₂ concentration. This may be a general circumstance where
393 there are large diurnal temperature extremes that rapidly change during the course of a day
394 and overnight, leading to lags in the timing of when temperature increases propagate down to
395 deeper soil layers.

396 Immediately prior to our visit to Konza Prairie (KONZ), that site that experienced a significant
397 rain event that led to wet soils that gradually dried out over the course of our time there.
398 This pulse of precipitation increased the soil CO₂ concentration at the top layer above the

399 concentrations in lower layers, leading to negative estimated flux values at the start of the field
400 sampling period. In this case it was only when the soil began to return to a baseline level that
401 the assumptions of the flux-gradient method were again met.

402 Both of the previous cases also provide context for the variable statistical comparisons between
403 field-measured soil fluxes and `neonSoilFlux` outputs (Figure 6). When considering systematic
404 deployment of this method across a measurement network, there are a number of independent
405 challenges that require careful consideration. There are clear tradeoffs between (1) accuracy of
406 modeled fluxes (defined here as closeness to field-measured F_S and the uncertainty reduction
407 factor ϵ), (2) precision (which could be defined by the signal to noise ratio), and (3) the
408 choice of the diffusivity model (Section 4.2.2) or flux computation method (Section 4.2.3). A
409 sensitivity analysis (Figure S2, Supplemental Information) found that flux output uncertainty
410 was dominated by measurement uncertainty (T_S , P , SWC , or CO_2) rather than by the diffusivity
411 method used to compute soil flux. Notably, the F_{110} method was least sensitive to measurement
412 uncertainty likely because it best aligns with the surface chamber measurement assumptions.

413 Finally, comparing the effects of different diffusivity estimation methods on the match between
414 modeled and measured fluxes (Figure 5) highlights the sensitivity of F_{ijk} to diffusivity. The
415 comparison between diffusivity estimates compared to field estimated diffusivity (Figure 7)
416 demonstrates that site parameters can dictate which measure of diffusivity is most likely to be
417 accurate in a given environmental context. Site-specific differences are largely a reflection of
418 differences in soil moisture across the sites (Table 1), as not all diffusivity estimation methods
419 incorporate soil moisture equivalently. While we here have compares two approaches to calculate
420 diffusivity (the Millington-Quirk and Marshall models), it may be valuable to evaluate other
421 diffusivity models (e.g. the Moldrup model; Moldrup et al. (1999)) as well. Ultimately the
422 choice of a particular diffusivity model could be determined based on knowledge of site-specific
423 evaluations or a set of these models could be used to generate a model ensemble average as a

⁴²⁴ means to trade precision for a more general approach.

⁴²⁵ **6.3 Recommendations for future method development**

⁴²⁶ The `neonSoilFlux` package provides several approaches to estimate soil flux using the gradient
⁴²⁷ method. We believe these approaches enable the software to be used across a range of site-
⁴²⁸ specific assumptions (Maier & Schack-Kirchner, 2014). We note, however, that this choice
⁴²⁹ can have a determinative approach on the calculated values. Ensemble averaging approaches
⁴³⁰ (Elshall et al., 2018; Raftery et al., 2005) may be one way to address this problem if the goal is
⁴³¹ to calculate fluxes using the same method at a diverse range of different sites. Two other ideas
⁴³² would be to apply machine learning algorithms (e.g. random forest) to generate a single flux
⁴³³ estimate across diverse sites, or using co-located estimates of net ecosystem carbon exchange
⁴³⁴ from eddy-flux towers to further constrain results or to assess soil flux results for plausibility
⁴³⁵ (Phillips et al., 2017).

⁴³⁶ These challenges notwithstanding, the method used here and made available in the
⁴³⁷ `neonSoilFlux` R package has the potential to produce nearly continuous estimates of flux
⁴³⁸ across all terrestrial NEON sites. These estimates are a significant improvement on available
⁴³⁹ approaches to constrain the portion of ecosystem respiration attributable to the soil. This, in
⁴⁴⁰ turn, also aids in our ability to understand the soil contribution to the net ecosystem flux
⁴⁴¹ measured at these sites using the co-located eddy flux towers.

⁴⁴² **7 Conclusions**

⁴⁴³ We used the R package `neonSoilFlux` to estimate soil CO₂ fluxes with the flux-gradient method
⁴⁴⁴ using data from buried soil sensors at NEON terrestrial sites. We compared the predicted

445 fluxes to those measured directly using a field-based closed chamber approach. Soil fluxes
446 from `neonSoilFlux` were broadly effective at producing estimates of flux comparable to those
447 measured in the field using a chamber-based technique. However `neonSoilFlux` outputs are
448 quite sensitive to a number of issues, including: missing data (and thus gap-filling of input
449 measurement datasets), the selection of soil depths used to best calculate the gradient (which
450 may vary between sites), and finally the choice of method used for estimating soil diffusivity.
451 The flexibility of the `neonSoilFlux` package allows the user to evaluate each of these issues
452 with site-specific knowledge and contexts. Future refinements and subsequent validation of
453 `neonSoilFlux` outputs will feed forward into evaluating soil carbon fluxes broader spatial scales
454 to enhance understanding of the ways in which soils across diverse ecosystems are responding
455 to a changing climate.

456 Sources Cited

- 457 Ayres, E., Reichle, R. H., Colliander, A., Cosh, M. H., & Smith, L. (2024). Validation of
458 Remotely Sensed and Modeled Soil Moisture at Forested and Unforested NEON Sites.
459 *IEEE Journal of Selected Topics in Applied Earth Observations and Remote Sensing*, 17,
460 14248–14264. <https://doi.org/10.1109/JSTARS.2024.3430928>
- 461 Baldocchi, D. (2014). Measuring fluxes of trace gases and energy between ecosystems and the
462 atmosphere - the state and future of the eddy covariance method. *Global Change Biology*,
463 20(12), 3600–3609. <https://doi.org/10.1111/gcb.12649>
- 464 Berenbaum, M. R., Carpenter, S. R., Hampton, S. E., Running, S. W., & Stanzione, D. C.
465 (2015). *Report from the NSF BIO Advisory Committee Subcommittee on NEON Scope*
466 *Impacts*.
- 467 Bond-Lamberty, B. (2018). New Techniques and Data for Understanding the Global Soil
468 Respiration Flux. *Earth's Future*, 6(9), 1176–1180. <https://doi.org/10.1029/2018EF000866>

- 469 Bond-Lamberty, B., Ballantyne, A., Berryman, E., Fluet-Chouinard, E., Jian, J., Morris, K.
470 A., Rey, A., & Vargas, R. (2024). Twenty Years of Progress, Challenges, and Opportunities
471 in Measuring and Understanding Soil Respiration. *Journal of Geophysical Research: Biogeosciences*, 129(2), e2023JG007637. <https://doi.org/10.1029/2023JG007637>
- 472
- 473 Bond-Lamberty, B., Christianson, D. S., Malhotra, A., Pennington, S. C., Sihi, D., AghaK-
474 ouchak, A., Anjileli, H., Altaf Arain, M., Armesto, J. J., Ashraf, S., Ataka, M., Baldocchi,
475 D., Andrew Black, T., Buchmann, N., Carbone, M. S., Chang, S.-C., Crill, P., Curtis, P.
476 S., Davidson, E. A., ... Zou, J. (2020). COSORE: A community database for continuous
477 soil respiration and other soil-atmosphere greenhouse gas flux data. *Global Change Biology*,
478 26(12), 7268–7283. <https://doi.org/10.1111/gcb.15353>
- 479 Bond-Lamberty, B., & Thomson, A. (2010). A global database of soil respiration data.
480 *Biogeosciences*, 7(6), 1915–1926. <https://doi.org/10.5194/bg-7-1915-2010>
- 481 Bond-Lamberty, B., Wang, C., & Gower, S. T. (2004). A global relationship between the
482 heterotrophic and autotrophic components of soil respiration? *Global Change Biology*,
483 10(10), 1756–1766. <https://doi.org/10.1111/j.1365-2486.2004.00816.x>
- 484 Bouma, T. J., & Bryla, D. R. (2000). On the assessment of root and soil respiration for soils of
485 different textures: Interactions with soil moisture contents and soil CO₂ concentrations.
486 *Plant and Soil*, 227(1), 215–221. <https://doi.org/10.1023/A:1026502414977>
- 487 Chen, H., & Tian, H.-Q. (2005). Does a General Temperature-Dependent Q10 Model of Soil
488 Respiration Exist at Biome and Global Scale? *Journal of Integrative Plant Biology*, 47(11),
489 1288–1302. <https://doi.org/10.1111/j.1744-7909.2005.00211.x>
- 490 Davidson, E. A., Janssens, I. A., & Luo, Y. (2006). On the variability of respiration in
491 terrestrial ecosystems: Moving beyond Q10. *Global Change Biology*, 12, 154–164. <https://doi.org/10.1111/j.1365-2486.2005.01065.x>
- 492
- 493 Desai, A. R., Murphy, B. A., Wiesner, S., Thom, J., Butterworth, B. J., Koupaei-Abyazani, N.,
494 Muttaqin, A., Paleri, S., Talib, A., Turner, J., Mineau, J., Merrelli, A., Stoy, P., & Davis,

- 495 K. (2022). Drivers of Decadal Carbon Fluxes Across Temperate Ecosystems. *Journal of*
496 *Geophysical Research: Biogeosciences*, 127(12), e2022JG007014. <https://doi.org/10.1029/2022JG007014>
- 497
- 498 Efron, B., & Tibshirani, R. J. (1994). *An Introduction to the Bootstrap*. Chapman and
499 Hall/CRC. <https://doi.org/10.1201/9780429246593>
- 500 Elshall, A. S., Ye, M., Pei, Y., Zhang, F., Niu, G.-Y., & Barron-Gafford, G. A. (2018). Relative
501 model score: A scoring rule for evaluating ensemble simulations with application to microbial
502 soil respiration modeling. *Stochastic Environmental Research and Risk Assessment*, 32(10),
503 2809–2819. <https://doi.org/10.1007/s00477-018-1592-3>
- 504 Falge, E., Baldocchi, D., Olson, R., Anthoni, P., Aubinet, M., Bernhofer, C., Burba, G.,
505 Ceulemans, R., Clement, R., Dolman, H., Granier, A., Gross, P., Grünwald, T., Hollinger,
506 D., Jensen, N.-O., Katul, G., Keronen, P., Kowalski, A., Lai, C. T., ... Wofsy, S. (2001).
507 Gap filling strategies for defensible annual sums of net ecosystem exchange. *Agricultural
508 and Forest Meteorology*, 107(1), 43–69. [https://doi.org/10.1016/S0168-1923\(00\)00225-2](https://doi.org/10.1016/S0168-1923(00)00225-2)
- 509 Farrance, I., & Frenkel, R. (2012). *Uncertainty of Measurement: A Review of the Rules
510 for Calculating Uncertainty Components through Functional Relationships*. *The Clinical
511 Biochemist Reviews*, 33(2), 49–75.
- 512 Friedlingstein, P., O’Sullivan, M., Jones, M. W., Andrew, R. M., Hauck, J., Landschützer,
513 P., Le Quéré, C., Li, H., Luijkx, I. T., Olsen, A., Peters, G. P., Peters, W., Pongratz,
514 J., Schwingshackl, C., Sitch, S., Canadell, J. G., Ciais, P., Jackson, R. B., Alin, S. R., ...
515 Zeng, J. (2025). Global Carbon Budget 2024. *Earth System Science Data*, 17(3), 965–1039.
516 <https://doi.org/10.5194/essd-17-965-2025>
- 517 Hamdi, S., Moyano, F., Sall, S., Bernoux, M., & Chevallier, T. (2013). Synthesis analysis
518 of the temperature sensitivity of soil respiration from laboratory studies in relation to
519 incubation methods and soil conditions. *Soil Biology and Biochemistry*, 58, 115–126.
520 <https://doi.org/10.1016/j.soilbio.2012.11.012>

- 521 Jackson, R. B., Lajtha, K., Crow, S. E., Hugelius, G., Kramer, M. G., & Piñeiro, G. (2017).
522 The Ecology of Soil Carbon: Pools, Vulnerabilities, and Biotic and Abiotic Controls.
523 *Annual Review of Ecology, Evolution and Systematics*, 48(Volume 48, 2017), 419–445.
524 <https://doi.org/10.1146/annurev-ecolsys-112414-054234>
- 525 Jian, J., Bailey, V., Dorheim, K., Konings, A. G., Hao, D., Shiklomanov, A. N., Snyder,
526 A., Steele, M., Teramoto, M., Vargas, R., & Bond-Lamberty, B. (2022). Historically
527 inconsistent productivity and respiration fluxes in the global terrestrial carbon cycle. *Nature
528 Communications*, 13(1), 1733. <https://doi.org/10.1038/s41467-022-29391-5>
- 529 Jian, J., Vargas, R., Anderson-Teixeira, K., Stell, E., Herrmann, V., Horn, M., Kholod, N.,
530 Manzon, J., Marchesi, R., Paredes, D., & Bond-Lamberty, B. (2021). A restructured and
531 updated global soil respiration database (SRDB-V5). *Earth System Science Data*, 13(2),
532 255–267. <https://doi.org/10.5194/essd-13-255-2021>
- 533 Jiang, J., Feng, L., Hu, J., Liu, H., Zhu, C., Chen, B., & Chen, T. (2024). Global soil
534 respiration predictions with associated uncertainties from different spatio-temporal data
535 subsets. *Ecological Informatics*, 82, 102777. <https://doi.org/10.1016/j.ecoinf.2024.102777>
- 536 Jobbágy, E. G., & Jackson, R. B. (2000). The Vertical Distribution of Soil Organic Carbon
537 and its Relation to Climate and Vegetation. *Ecological Applications*, 10(2), 423–436.
538 [https://doi.org/10.1890/1051-0761\(2000\)010%5B0423:TVDOSO%5D2.0.CO;2](https://doi.org/10.1890/1051-0761(2000)010%5B0423:TVDOSO%5D2.0.CO;2)
- 539 Jurasinski, G., Koebisch, F., Guenther, A., & Beetz, S. (2022). *Flux: Flux Rate Calculation
540 from Dynamic Closed Chamber Measurements*.
- 541 Liu, K., Li, X., Wang, S., & Zhang, H. (2023). A robust gap-filling approach for European
542 Space Agency Climate Change Initiative (ESA CCI) soil moisture integrating satellite
543 observations, model-driven knowledge, and spatiotemporal machine learning. *Hydrology
544 and Earth System Sciences*, 27(2), 577–598. <https://doi.org/10.5194/hess-27-577-2023>
- 545 Lunch, C., Laney, C., Mietkiewicz, N., Sokol, E., Cawley, K., & Network), N. (National. E. O.
546 (2025). *neonUtilities: Utilities for Working with NEON Data*.

- 547 Luo, Y., Ogle, K., Tucker, C., Fei, S., Gao, C., LaDeau, S., Clark, J. S., & Schimel, D. S. (2011).
548 Ecological forecasting and data assimilation in a data-rich era. *Ecological Applications*,
549 21(5), 1429–1442. <https://doi.org/10.1890/09-1275.1>
- 550 Maier, M., & Schack-Kirchner, H. (2014). Using the gradient method to determine soil gas
551 flux: A review. *Agricultural and Forest Meteorology*, 192–193, 78–95. <https://doi.org/10.1016/j.agrformet.2014.03.006>
- 553 Mariethoz, G., Linde, N., Jougnot, D., & Rezaee, H. (2015). Feature-preserving interpolation
554 and filtering of environmental time series. *Environmental Modelling & Software*, 72, 71–76.
555 <https://doi.org/10.1016/j.envsoft.2015.07.001>
- 556 Marshall, T. J. (1959). The Diffusion of Gases Through Porous Media. *Journal of Soil Science*,
557 10(1), 79–82. <https://doi.org/10.1111/j.1365-2389.1959.tb00667.x>
- 558 Millington, R. J., & Shearer, R. C. (1971). Diffusion in aggregated porous media. *Soil Science*,
559 111(6), 372–378.
- 560 Moffat, A. M., Papale, D., Reichstein, M., Hollinger, D. Y., Richardson, A. D., Barr, A. G.,
561 Beckstein, C., Braswell, B. H., Churkina, G., Desai, A. R., Falge, E., Gove, J. H., Heimann,
562 M., Hui, D., Jarvis, A. J., Kattge, J., Noormets, A., & Stauch, V. J. (2007). Comprehensive
563 comparison of gap-filling techniques for eddy covariance net carbon fluxes. *Agricultural and
564 Forest Meteorology*, 147(3), 209–232. <https://doi.org/10.1016/j.agrformet.2007.08.011>
- 565 Moldrup, P., Olesen, T., Yamaguchi, T., Schjønning, P., & Rolston, D. E. (1999). Modeling
566 diffusion and reaction in soils: 9. The Buckingham-Burdine-Campbell equation for gas
567 diffusivity in undisturbed soil. *Soil Science*, 164(2), 75.
- 568 NEON. (2024a). *Barometric pressure (DP1.00004.001)*. National Ecological Observatory
569 Network (NEON). <https://doi.org/10.48443/RT4V-KZ04>
- 570 NEON. (2024b). *Soil CO₂ concentration (DP1.00095.001)*. National Ecological Observatory
571 Network (NEON). <https://doi.org/10.48443/E7GR-6G94>
- 572 NEON. (2024c). *Soil physical and chemical properties, Megapit (DP1.00096.001)*. National

- 573 Ecological Observatory Network (NEON). <https://doi.org/10.48443/S6ND-Q840>
- 574 NEON. (2024d). *Soil temperature (DP1.00041.001)*. National Ecological Observatory Network
575 (NEON). <https://doi.org/10.48443/Q24X-PW21>
- 576 NEON. (2024e). *Soil water content and water salinity (DP1.00094.001)*. National Ecological
577 Observatory Network (NEON). <https://doi.org/10.48443/A8VY-Y813>
- 578 Norman, J. M., Kucharik, C. J., Gower, S. T., Baldocchi, D. D., Crill, P. M., Rayment,
579 M., Savage, K., & Striegl, R. G. (1997). A comparison of six methods for measuring
580 soil-surface carbon dioxide fluxes. *Journal of Geophysical Research: Atmospheres*, 102(D24),
581 28771–28777. <https://doi.org/10.1029/97JD01440>
- 582 Pedersen, A. R. (2024). *HMR: Flux Estimation with Static Chamber Data*.
- 583 Phillips, C. L., Bond-Lamberty, B., Desai, A. R., Lavoie, M., Risk, D., Tang, J., Todd-Brown,
584 K., & Vargas, R. (2017). The value of soil respiration measurements for interpreting and
585 modeling terrestrial carbon cycling. *Plant and Soil*, 413(1), 1–25. <https://doi.org/10.1007/s11104-016-3084-x>
- 587 Raftery, A. E., Gneiting, T., Balabdaoui, F., & Polakowski, M. (2005). *Using Bayesian Model
588 Averaging to Calibrate Forecast Ensembles*. <https://doi.org/10.1175/MWR2906.1>
- 589 Rheault, K., Christiansen, J. R., & Larsen, K. S. (2024). goFlux: A user-friendly way to
590 calculate GHG fluxes yourself, regardless of user experience. *Journal of Open Source
591 Software*, 9(96), 6393. <https://doi.org/10.21105/joss.06393>
- 592 Sallam, A., Jury, W. A., & Letey, J. (1984). Measurement of Gas Diffusion Coefficient under
593 Relatively Low Air-filled Porosity. *Soil Science Society of America Journal*, 48(1), 3–6.
594 <https://doi.org/10.2136/sssaj1984.03615995004800010001x>
- 595 Shao, J., Zhou, X., Luo, Y., Li, B., Aurela, M., Billesbach, D., Blanken, P. D., Bracho, R.,
596 Chen, J., Fischer, M., Fu, Y., Gu, L., Han, S., He, Y., Kolb, T., Li, Y., Nagy, Z., Niu, S.,
597 Oechel, W. C., ... Zhang, J. (2015). Biotic and climatic controls on interannual variability
598 in carbon fluxes across terrestrial ecosystems. *Agricultural and Forest Meteorology*, 205,

- 599 11–22. <https://doi.org/10.1016/j.agrformet.2015.02.007>
- 600 Shao, P., Zeng, X., Moore, D. J. P., & Zeng, X. (2013). Soil microbial respiration from
601 observations and Earth System Models. *Environmental Research Letters*, 8(3), 034034.
602 <https://doi.org/10.1088/1748-9326/8/3/034034>
- 603 Sihi, D., Gerber, S., Inglett, P. W., & Inglett, K. S. (2016). Comparing models of microbial–
604 substrate interactions and their response to warming. *Biogeosciences*, 13(6), 1733–1752.
605 <https://doi.org/10.5194/bg-13-1733-2016>
- 606 Tang, J., Baldocchi, D. D., Qi, Y., & Xu, L. (2003). Assessing soil CO₂ efflux using continuous
607 measurements of CO₂ profiles in soils with small solid-state sensors. *Agricultural and Forest
608 Meteorology*, 118(3), 207–220. [https://doi.org/10.1016/S0168-1923\(03\)00112-6](https://doi.org/10.1016/S0168-1923(03)00112-6)
- 609 Tang, J., Misson, L., Gershenson, A., Cheng, W., & Goldstein, A. H. (2005). Continuous
610 measurements of soil respiration with and without roots in a ponderosa pine plantation
611 in the Sierra Nevada Mountains. *Agricultural and Forest Meteorology*, 132(3), 212–227.
612 <https://doi.org/10.1016/j.agrformet.2005.07.011>
- 613 Taylor, J. R. (2022). *An Introduction to Error Analysis: The Study of Uncertainties in Physical
614 Measurements, Third Edition* (3rd ed.). University Science Press.
- 615 Wilson, S. J., Bond-Lamberty, B., Noyce, G., Bittencourt Peixoto, R., & Megonigal, J. P.
616 (2024). Fluxfinder: An R Package for Reproducible Calculation and Initial Processing
617 of Greenhouse Gas Fluxes From Static Chamber Measurements. *Journal of Geophysical
618 Research: Biogeosciences*, 129(11), e2024JG008208. <https://doi.org/10.1029/2024JG008208>
- 619 Yan, Z., Bond-Lamberty, B., Todd-Brown, K. E., Bailey, V. L., Li, S., Liu, C., & Liu, C. (2018).
620 A moisture function of soil heterotrophic respiration that incorporates microscale processes.
621 *Nature Communications*, 9(1), 2562. <https://doi.org/10.1038/s41467-018-04971-6>
- 622 Yan, Z., Liu, C., Todd-Brown, K. E., Liu, Y., Bond-Lamberty, B., & Bailey, V. L. (2016).
623 Pore-scale investigation on the response of heterotrophic respiration to moisture conditions
624 in heterogeneous soils. *Biogeochemistry*, 131(1), 121–134. <https://doi.org/10.1007/s10533-016-0333-0>

- 625 016-0270-0
- 626 Zhang, R., Kim, S., Kim, H., Fang, B., Sharma, A., & Lakshmi, V. (2023). Temporal Gap-Filling
627 of 12-Hourly SMAP Soil Moisture Over the CONUS Using Water Balance Budgeting. *Water*
628 *Resources Research*, 59(12), e2023WR034457. <https://doi.org/10.1029/2023WR034457>
- 629 Zhao, J. (2019). FluxCalR: A R package for calculating CO₂ and CH₄ fluxes from static
630 chambers. *Journal of Open Source Software*, 4(43), 1751. <https://doi.org/10.21105/joss.01751>
- 632 Zobitz, J., Ayres, E., O'Rourke, K., Werbin, Z., Lee, L., Abdi, R., Mehmeti, D., & Xiong, L.
633 (2024). *neonSoilFlux: Compute Soil Carbon Fluxes for the National Ecological Observatory*
634 *Network Sites*.